293(W) cells, the dimer/monomer ratio was increased ~40% by the addition of EGF. Addition of EGF slightly increased the dimer/monomer ratio (~20%) in the 293(D) cells.

We investigated the dimerization and phosphorylation status of EGFR in the EGFR-transfected cell lines under serum-starved conditions (Fig. 2*B*). The transfected cells were exposed by EGF (10 ng/ml for 10 min) after serum starvation for 24 h. No expression of EGFR dimer or monomer was detected in the 293(M) cells. Addition of EGF resulted in an increase in dimerized and phosphorylated EGFR in the 293(W) cells. Dimerization and phosphorylation of the deletional EGFR were detected in the 293(D) cells in the absence of EGF after serum starvation. Expression of dimerized EGFR in the 293(D) cells was unchanged by EGF stimulation. These findings demonstrated that the deletional mutant EGFR was constitutively dimerized and phosphorylated without any ligand stimulation even under starved conditions and are consistent with the results under nonstarved conditions (Fig. 2*A*). The ratio of dimerized to monomeric EGFR in 293(W) and 293(D) cells was analyzed densitometrically under serum-starved conditions (Fig. 2*B*, right). The dimer/monomer ratio in the 293(W) cells was markedly increased (~3 fold) by addition of EGF. Under unstimulated conditions, the dimer/monomer ratio of the 293(D) cells was higher than that of the 293(W) cells, and the ratio was unchanged by addition of EGF.

These results suggest that the cells expressing the wild-type of EGFR responded to EGF for their dimerization and phosphorylation and that the deletion mutant of EGFR was dimerized and phosphorylated constitutively without any ligand stimulation.

Phosphorylation of EGFR, p44/42 MAPK, and AKT in the EGFR-transfected 293 cells

The p44/42 MAPK and AKT are major downstream targets of EGFR. We examined the phosphorylation status of p44/42 MAPK and AKT with EGF addition in the transfectants. The transfected cells were treated with EGF (10 ng/ml) for 10 min under nonstarved conditions (Fig. 3*A*). The phosphorylation levels of EGFR in the 293(D) cells were higher without any ligand stimulation than that of the 293(W) cells. Phospho-EGFR in the 293(W) cells was increased after EGF stimulation. These findings are consistent with Fig. 2. Even under unstimulated conditions, increased phosphorylation of p44/42 MAPK and AKT was observed in the 293(D) cells. In the 293(W) cells, increased phosphorylation of p44/42 MAPK and AKT was observed with the addition of EGF especially p44/42 MAPK was remarkably phosphorylated. On the other hand, in the 293(D) cells, phosphorylation of p44/42 MAPK and AKT was not increased with the addition of EGF. We quantified the phosphorylation levels of p44/42 MAPK and AKT densitometrically in the transfectants in response to EGF. The addition of EGF increased phosphorylation of p44/42 MAPK in the 293(M) cells (~3.4 fold) and in the 293(W) cells (~2.5 fold) (Fig. 3*B*), suggesting no difference in response in regard to p44/42 MAPK to EGF. Increased phosphorylation of AKT in the 293(M) cells (~2.1 fold) and in the 293(W) cells (~1.3 fold) was observed. By contrast, EGF decreased the phosphorylation of p44/42 MAPK and AKT in the 293(D) cells ~30% and ~20% (Fig. 3*C*). These findings suggest that the p44/42 MAPK and AKT pathways are activated in cells expressing the deletional EGFR without ligand stimulation.

Next, we examined the dose-dependent response of EGFR status in the transfected cells to the other ligands, TGF-α, and HB-EGF, after serum starvation (Fig. 4). The hyperphosphorylated EGFR in the 293(D) cells was unchanged by stimulation with these ligands either. By contrast, a dose-dependent increase in EGFR phosphorylation was observed in the 293(W) cells in response to stimulation by TGF-α and HB-EGF. Both HB-EGF and EGF strongly increased EGFR

phosphorylation in the 293(W) cells compared with TGF-α. We also examined the downstream in response to these ligands. In the 293(W) cells, increased phosphorylation of p44/42 MAPK and AKT was observed in response to addition of the ligands (EGF, TGF-α, and HB-EGF). p44/42 MAPK was markedly phosphorylated by the ligands. In the 293(D) cells, addition of ligands further increased p44/42 MAPK phosphorylation. The AKT phosphorylation in the 293(D) cells was unchanged by stimulation with these ligands. These findings are consistent with the data in Fig. 3*A*, and suggest that the p44/42 MAPK and AKT pathways are both activated in cells constitutively expressing the deletional EGFR.

Effect of gefitinib on phosphorylation of EGFR, p44/42 MAPK, and AKT in the EGFR-transfected 293 cells

Previously, we demonstrated that 293(D) cells were hypersensitive to EGFR-targeted tyrosine kinase inhibitors such as gefitinib and ZD6474, as compared with 293(W) cells (6). To examine the specific action of these tyrosine kinase inhibitors on deletional EGFR signal transduction, we exposed the 293 transfectants to gefitinib, and its cellular response was examined under nonstarved conditions with an immunoblot analysis (Fig. 5*A*). In the 293(W) cells, phosphorylation of p44/42 MAPK was not inhibited by exposure to a low dose of gefitinib (0.01 μM) but phosphorylation of AKT was inhibited by exposure to gefitinib (0.01 μM). In contrast, exposure to gefitinib decreased phospho-EGFR in the 293(D) cells that are hypersensitive to gefitinib. Phosphorylation of AKT was completely inhibited by 0.01 μM gefitinib exposure, while the inhibition of p44/42 MAPK phosphorylation was not remarkable in the 293(D) cells. The effect of 0.01 μM gefitinib on phosphorylated p44/42 MAPK and AKT in the transfectents measured densitometrically. p44/42 MAPK phosphorylation in the 293(M) and 293(W) cells was unaltered by gefitinib exposure for 3 h, but it decreased in the 293(D) cells (~20%) (Fig. 5*B*). Gefitinib increased phosphorylation of AKT ~1.3 fold in the 293(M) cells. Gefitinib inhibited AKT phosphorylation was ~70% in the 293(W) cells, and decreased it ~99% in the 293(D) cells (Fig. 5*C*).

We examined the dose-dependent effect of gefitinib (0.02, 0.2, 2 μM) on EGFR and its downstream signaling in all of the transfectants under serum-starved conditions. Phosphorylation of EGFR was not detected in the 293(W) cells under the 24 h serum-starved conditions, and gefitinib had no effect on it (Fig. 6*A*). Hyperphosphorylation of EGFR was dose dependently inhibited by gefitinib in the 293(D) cells. p44/42 MAPK and AKT were slightly phosphorylated in the 293(W) cells, and their degree of phosphorylation was unaltered by exposure to gefitinib. By contrast, gefitinib dose-dependently decreased phosphorylation of p44/42 MAPK, and AKT in the 293(D) cells. Under EGF stimulation (Fig. 6*B*), gefitinib dose-dependently decreased phosphorylation of EGFR, p44/42 MAPK, and AKT in the 293(W) cells. Phosphorylation of EGFR in the 293(D) cells was completely inhibited by a low concentration of gefitinib (0.02 μM), and phosphorylation of p44/42 MAPK and AKT was dose-dependently inhibited by gefitinib. A low concentration of gefitinib inhibited EGFR phosphorylation and its signal in the 293(D) cells under serum-starved conditions. The phosphorylation of EGFR (and its signal) induced by EGF-addition in the 293(W) cells was inhibited by gefitinib dose dependently.

These data suggest that gefitinib inhibited the AKT signaling pathway more strongly than the p44/42 MAPK signaling pathway in the cells expressing the deletional mutant EGFR.

Response to EGF stimulation in the EGFR-transfected 293 cells

We performed the quantitative phosphoprotein analysis in the 293(W) and 293(D) cells by a beads-based multiplex assay. Downstream from the reaction, we monitored the phosphorylation status of p44/42 MAPK, JNK, and p38 MAPK. We also examined the phosphorylation status of ATF-2 that is located downstream of the MAPK pathway, IκB-α that is a member of the AKT pathway, and STAT-3 that is found downstream of the other signaling pathway. Even under unstimulated conditions, EGFR was hyperphosphorylated in the 293(D) cells but not in the 293(W) cells (Fig. 7*A*). Increased phosphorylation of EGFR was observed in the 293(W) cells (~40 fold), but the phosphorylation of EGFR in the 293(W) cells was much lower than that of the deletional EGFR in the 293(D) cells. IκB-α phosphorylation in the transfected cells was as low as in the HeLa cells, which was used as a negative control (Fig. 7*B*). Under unstimulated conditions, phosphorylation of p44/42 MAPK was greater in the 293(D) cells than in the 293(W) cells (~3 fold) (Fig. 7*C*). A large increase in phosphorylation of p44/42 MAPK in response to the addition of EGF was observed in the 293(W) cells (~15 fold), and a smaller increase was observed in the 293(D) cells (~3.5 fold). These differences in phosphorylated p44/42 MAPK in the 293(W) and 293(D) cells detected in the beads-based multiplex assay are consistent with the result of immunoblotting (Fig. 4). ATF-2 was phosphorylated in the 293(W) cells (~1.5 fold) and 293(D) cells (~1.7 fold) by addition of EGF (Fig. 7*D*). By contrast, the JNK in the 293(W) cells was phosphorylated by addition of EGF (~2 fold), but not phosphorylated in the 293(D) cells (Fig. 7*E*). Phosphorylation of p38 MAPK and STAT-3 was not detected in either type of cell (data not shown). These findings suggest that the p44/42 MAPK and AKT pathways are both phosphorylated without any ligand stimulation in the cells expressing the deletional mutant EGFR.

Response to EGF stimulation in PC-9 cells intrinsically expressing deletional EGFR

The hyperphosphorylation and increased dimerization of deletional EGFR has been demonstrated by ectopic expression of deletional EGFR. To examine whether this phenomenon is also observed in the lung cancer cells intrinsically expressing deletional EGFR, we monitored the phosphorylation of EGFR and its related molecules in the PC-9 cells as compared with the A549 cells. The PC-9 cells and A549 cells express the deletional and wild-type EGFR, respectively. PC-9 cells also express a small amount of wild-type EGFR, and so these cell lines mimic the 293(D) cells. We examined the phosphorylation of EGFR and its downstream signaling molecules in these cells by immunoblotting (Fig. 8*A*). Increased phosphorylation of EGFR was observed in the PC-9 cells even under unstimulated conditions, but not in the A549 cells. The addition of EGF markedly increased the EGFR phosphorylation in the A549 cells compared with the PC-9 cells. Under unstimulated conditions, p44/42 MAPK, and AKT were more phosphorylated in the PC-9 cells than in the A549 cells. Increased phosphorylation of p44/42 MAPK and AKT was observed in the A549 cells after addition of EGF, and p44/42 MAPK was markedly phosphorylated. A small increase in phosphorylation of p44/42 MAPK and AKT was observed in the PC-9 cells in response to the addition of EGF. The increased phosphorylation of IκB-α in the PC-9 cells was observed even under unstimulated conditions. The addition of EGF increased the phosphorylation of IκB-α in the A549 cells but did not alter it in the PC-9 cells. These findings suggest a difference in reactivity to the EGF stimulation between the A549 and PC-9 cells.

Next, examination was performed by a beads-based mulitiplex assay. Increased phosphorylation of EGFR was observed in the PC-9 cells, even under unstimulated conditions, but not in the A549 cells (Fig. 8*B*). These findings are consistent with the results of immunoblotting. EGFR

phosphorylation was markedly increased in the A549 cells (~100-fold), and to a lesser extent increased in the PC-9 cells (~1.4-fold). IκB-α was phosphorylated in the PC-9 cells in the absence of EGF stimulation (Fig. 8*C*), suggesting that the AKT pathway, including IκB-α, was activated in the PC-9 cells expressing deletional EGFR, compared with A549 cells. p44/42 MAPK and ATF-2 were phosphorylated without EGF stimulation in the PC-9 cells compared with the A549 cells (Fig. 8*D* and *E*). A large increase in phosphorylation of p44/42 MAPK and ATF-2 was observed in the A549 cells (~13 fold and ~4.3 fold), and a smaller increase was observed in the PC-9 cells (~3.5-fold and ~1.7-fold). JNK was not phosphorylated in either the A549 or the PC-9 cells. Phosphorylation of JNK in response to EGF stimulation was detected in the A549 cells (~2.6-fold), but not in the PC-9 cells (Fig. 8*F*). No phosphorylation of p38 MAPK and STAT-3 was detected in either cell line (data not shown). These differences in phosphoproteins in the A549 and PC-9 cells are consistent with the results of the beads-based multiplex assay in the EGFR-transfected cells (293(W) and 293(D)) (Fig. 7).

To determine whether there was a significant difference between unstimulated and EGF-stimulated conditions, a statistical analysis was performed using the *t* test. There were significant differences between increased phospho-EGFR, phospho-p44/42 MAPK, phospho-ATF-2, and phospho-JNK ($P>0.01$) in the A549 cells under unstimulated and EGF-stimulated conditions. There were also significant differences in the increased phospho-EGFR, phospho-p44/42 MAPK, phospho-ATF-2, and phospho-IκB-α ($P>0.01$) in the PC-9 cells. The fact that phosphorylation of EGFR, p44/42 MAPK, and ATF-2 in the PC-9 cells is still modulated by EGF stimulation cannot be ignored. This pathway is considered to be preferentially regulated by wild-type EGFR.

DISCUSSION

Previous studies have demonstrated that mutational EGFR is a major factor against determining gefitinib sensitivity. We analyzed the characteristics of deletional EGFR with cells expressing deletional EGFR.

In Fig. 3, phosphorylation of p44/42 MAPK and AKT was increased by EGF in the 293(M) cells, although the EGFR was not overexpressed in these cells. There is a rich cross-talk among the ErbB family that regulates the cellular effects mediated by these receptors. However, ErbB-2 (HER2), ErbB-3 (HER3), and ErbB-4 (HER4) are not expressed, and intrinsic EGFR was weakly expressed in the 293 cells (15). Activation of p44/42 MAPK and AKT in response to EGF might be mediated by the intrinsic EGFR. On the other hand, constitutive activation of EGFR and its downstream pathway is due to the mutant EGFR in the 293(D) cells, suggesting that the mutant EGFR shows a dominant phenotype.

In Fig. 3, p44/42 MAPK and AKT were activated under unstimulated conditions in the 293(D) cells. In these transfectants, EGF did not enhance the phosphorylation of p44/42 MAPK and AKT in contrast to those in the 293(W) cells. The phosphorylation of AKT in these cells seems to be decreased by the addition of EGF (Fig. 3*A*). It can be speculated that EGF negatively regulated the activation of mutant EGFR as a feedback mechanism. It is uncertain whether EGF itself negatively regulates the mutant EGFR. Although the mechanism of this phenomenon remains uncertain, a feedback mechanism might be postulated as a possible explanation. It was reported that leucine-rich repeats and immunoglobulin-like domains 1 (LIRG1) is a negative regulator of EGFR (16) and its transcription was up-regulated by EGF stimulation and caused consequently

degradation of EGFR. Thus the feedback mechanisms, including that mediated by LIRG1, should be clarified in the future study.

The 293(D) cells transfected with deletional EGFR were hypersensitive to the growth-inhibitory effect of EGFR tyrosine kinase inhibitor, including gefitinib (6). AKT phosphorylation was completely suppressed by 0.01 μM gefitinib in the 293(D) cells (Fig. 5). It is suggested that deletional EGFR signaling inclines toward the AKT pathways, and this is correlated with cellular sensitivity to gefitinib. The response to gefitinib in the 293(M) cells cannot be ignored. We speculate that the difference in cell response to gefitinib may be attributable to cell dependency on EGFR in the 293(M), 293(W), and 293(D) cells. Since the 293(W) and 293(D) cells seem to be largely dependent on EGFR, therefore, gefitinib effectively inhibited the AKT phosphorylation in these cells. Cell growth in 293(M) cells, on the other hand, is regulated by other signaling pathways. Then the MAPK and AKT pathways did not respond to gefitinib. In addition, the PC-9 cells intrinsically expressing deletional EGFR were also hypersensitive to gefitinib (11, 17), and the AKT pathway was more sensitively inhibited by gefitinib as compared with p44/42 MAPK pathway (18). These findings are consistent with the evidence seen in the 293(D) cells. The altered downstream pathway in the cells expressing other types of mutant EGFR was previously reported. The L858R and delL747-P753insS were basically unphosphorylated and these mutants were markedly phosphorylated compared with wild-type EGFR by ligand stimulation (4, 5). Activated AKT signaling pathways, but not MAPK pathway was observed in the transfectants of L858R and delL747-P753insS. Taken together, preferential activation of AKT pathway was commonly observed between these EGFR mutant cells. On the other hand, there were some differences between delE746-A750, L858R, and delL747-P753insS; constitutive active in delE746-A750 vs. hyperresponse to ligand stimulation in L858R and delL747-P753insS. These EGFR mutations except for T790M are considered to be "gain of function," although detailed differential function will be clarified in future studies.

We examined the phosphorylation status of EGFR and its downstream events in PC-9 cells intrinsically expressing deletional mutant EGFR in addition to the ectopic expression system. However, the PC-9 cells also express low levels of wild-type of EGFR. It can thus be considered that these cells mimic the 293(D) cells. In the PC-9 cells, IκB-α is activated. IκB-α binds to NF-κB and suppresses this function (19). Kapoor reported that NF-κB activating signal from EGFR is mediated by the PI3-kinase/AKT pathway (20). We used immunoblotting to investigate the phosphorylation of AKT in the PC-9 cells after EGF stimulation. Increased phosphorylation of AKT was induced even under unstimulated conditions and considered that the activation (or phosphorylation) of IκB-α occurred via the AKT pathway machinery. Therefore, the phosphorylation of IκB-α is due to the activation of the AKT pathway in the PC-9 cells.

In the PC-9 cells, increased phosphorylation of p44/42 MAPK and ATF-2 (21, 22) was detected with the addition of EGF. In addition, phosphorylation of IκB-α was also increased by the ligand stimulation in the PC-9 cells, suggesting that this signaling pathway might be mediated by wild-type of EGFR.

We demonstrated that deletional EGFR was hyperphosphorylated and dimerized in a steady state in the 293(D) cells. This mutant is considered to be constitutively active. The activation mutation in EGFR is consistent with that of the c-KIT mutation in GIST that is a target for gleevec (23). The c-KIT mutations in GIST have also been reported as gain-of-function mutations (24). The role of

mutant EGFR and its function in transformation activity and carcinogenesis requires clarification in future studies.

Downstream of the signaling pathway, p44/42 MAPK and AKT pathways are activated in the 293(D) cells, but the AKT pathway was more strongly suppressed by gefitinib. Therefore, the AKT pathway must interact with cellular hypersensitivity to the EGFR targeted tyrosine kinase inhibitor in cells expressing deletional mutant EGFR.

In this study, we focused on the short, in-frame deletional mutant (E746_A750del). Now more than 30 types of mutation have been reported in clinical lung cancer specimens. In the next step, we will examine the biological function of other types of mutants of EGFR differentially, with the aim of selecting clinically meaningful mutations.

ACKNOWLEDGMENTS

This work was supported by funds for the Third Term Comprehensive 10-Year Strategy for Cancer Control and a Grant-in-Aid for Scientific Research from the Ministry of Education, Culture, Sports, Science and Technology of Japan (12217165).

REFERENCES

1. Yarden, Y., and Sliwkowski, M. X. (2001) Untangling the ErbB signalling network. *Nat. Rev. Mol. Cell Biol.* **2**, 127–137

2. Tanner, K. G., and Kyte, J. (1999) Dimerization of the extracellular domain of the receptor for epidermal growth factor containing the membrane-spanning segment in response to treatment with epidermal growth factor. *J. Biol. Chem.* **274,** 35,985–35,990

3. Paez, J. G., Janne, P. A., Lee, J. C., Tracy, S., Greulich, H., Gabriel, S., Herman, P., Kaye, F. J., Lindeman, N., Boggon, T. J., et al. (2004) EGFR mutations in lung cancer: correlation with clinical response to gefitinib therapy. *Science* **304,** 1497–1500

4. Lynch, T. J., Bell, D. W., Sordella, R., Gurubhagavatula, S., Okimoto, R. A., Brannigan, B. W., Harris, P. L., Haserlat, S. M., Supko, J. G., Haluska, F. G., et al. (2004) Activating mutations in the epidermal growth factor receptor underlying responsiveness of non-small-cell lung cancer to gefitinib. *N. Engl. J. Med.* **350,** 2129–2139

5. Sordella, R., Bell, D. W., Haber, D. A., and Settleman, J. (2004) Gefitinib-sensitizing EGFR mutations in lung cancer activate anti-apoptotic pathways. *Science* **305,** 1163–1167

6. Arao, T., Fukumoto, H., Takeda, M., Tamura, T., Saijo, N., and Nishio, K. (2004) Small in-frame deletion in the epidermal growth factor receptor as a target for ZD6474. *Cancer Res.* **64,** 9101–9104

7. Tracy, S., Mukohara, T., Hansen, M., Meyerson, M., Johnson, B. E., and Janne, P. A. (2004) Gefitinib induces apoptosis in the EGFRL858R non-small-cell lung cancer cell line H3255. *Cancer Res.* **64,** 7241–7244

8. Chang, L., and Karin, M. (2001) Mammalian MAP kinase signalling cascades. *Nature* **410,** 37–40

9. Kawamura-Akiyama, Y., Kusaba, H., Kanzawa, F., Tamura, T., Saijo, N., and Nishio, K. (2002) Non-cross resistance of ZD0473 in acquired cisplatin-resistant lung cancer cell lines. *Lung Cancer* **38,** 43–50

10. Nishio, K., Arioka, H., Ishida, T., Fukumoto, H., Kurokawa, H., Sata, M., Ohata, M., and Saijo, N. (1995) Enhanced interaction between tubulin and microtubule-associated protein 2 via inhibition of MAP kinase and CDC2 kinase by paclitaxel. *Int. J. Cancer* **63,** 688–693

11. Koizumi, F., Shimoyama, T., Saijo, N., and Nishio, K. Establishment of a human non-small cell lung cancer cell line resistant to gefitinib. *Int. J. Cancer* **116,** 36–44

12. Koizumi, F., Kanzawa, F., Ueda, Y., Koh, Y., Tsukiyama, S., Taguchi, F., Tamura, T., Saijo, N., and Nishio, K. (2004) Synergistic interaction between the EGFR tyrosine kinase inhibitor gefitinib ("Iressa") and the DNA topoisomerase I inhibitor CPT-11 (irinotecan) in human colorectal cancer cells. *Int. J. Cancer* **108,** 464–472

13. Fulton, R. J., McDade, R. L., Smith, P. L., Kienker, L. J., and Kettman, J. R., Jr. (1997) Advanced multiplexed analysis with the FlowMetrix system. *Clin. Chem.* **43,** 1749–1756

14. Gingrich, J. C., Davis, D. R., and Nguyen, Q. (2000) Multiplex detection and quantitation of proteins on western blots using fluorescent probes. *Biotechniques* **29,** 636–642

15. Chan, S. D., Antoniucci, D. M., Fok, K. S., Alajoki, M. L., Harkins, R. N., Thompson, S. A., and Wada, H. G. (1995) Heregulin activation of extracellular acidification in mammary carcinoma cells is associated with expression of HER2 and HER3. *J. Biol. Chem.* **270,** 22,608–22,613

16. Gur, G., Rubin, C., Katz, M., Amit, I., Citri, A., Nilsson, J., Amariglio, N., Henriksson, R., Rechavi, G., Hedman, H., et al. (2004) LRIG1 restricts growth factor signaling by enhancing receptor ubiquitylation and degradation. *EMBO J.* **23,** 3270–3281

17. Naruse, I., Fukumoto, H., Saijo, N., and Nishio, K. (2002) Enhanced anti-tumor effect of trastuzumab in combination with cisplatin. *Jpn. J. Cancer Res.* **93,** 574–581

18. Ono, M., Hirata, A., Kometani, T., Miyagawa, M., Ueda, S., Kinoshita, H., Fujii, T., and Kuwano, M. (2004) Sensitivity to gefitinib (Iressa, ZD1839) in non-small cell lung cancer cell lines correlates with dependence on the epidermal growth factor (EGF) receptor/extracellular signal-regulated kinase 1/2 and EGF receptor/AKT pathway for proliferation. *Mol. Cancer Ther.* **3,** 465–472

19. Baeuerle, P. A., and Baltimore, D. (1988) I kappa B: a specific inhibitor of the NF-kappa B transcription factor. *Science* **242,** 540–546

20. Kapoor, G. S., Zhan, Y., Johnson, G. R., and O'Rourke, D. M. (2004) Distinct domains in the SHP-2 phosphatase differentially regulate epidermal growth factor receptor/NF-kappaB activation through Gab1 in glioblastoma cells. *Mol. Cell. Biol.* **24,** 823–836

21. Gupta, S., Campbell, D., Derijard, B., and Davis, R. J. (1995) Transcription factor ATF2 regulation by the JNK signal transduction pathway. *Science* **267,** 389–393

22. Morton, S., Davis, R. J., and Cohen, P. (2004) Signaling pathways involved in multisite phosphorylation of the transcription factor ATF-2. *FEBS Lett.* **572,** 177–183

23. Hirota, S., Isozaki, K., Moriyama, Y., Hashimoto, K., Nishida, T., Ishiguro, S., Kawano, K., Hanada, M., Kurata, A., Takeda, M., et al. (1998) Gain-of-function mutations of c-kit in human gastrointestinal stromal tumors. *Science* **279,** 577–580

24. Tarn, C., Merkel, E., Canutescu, A. A., Shen, W., Skorobogatko, Y., Heslin, M. J., Eisenberg, B., Birbe, R., Patchefsky, A., Dunbrack, R., et al. (2005) Analysis of KIT mutations in sporadic and familial gastrointestinal stromal tumors: therapeutic implications through protein modeling. *Clin. Cancer Res.* **11,** 3668–3677

Received April 23, 2005; accepted October 25, 2005

Fig. 1

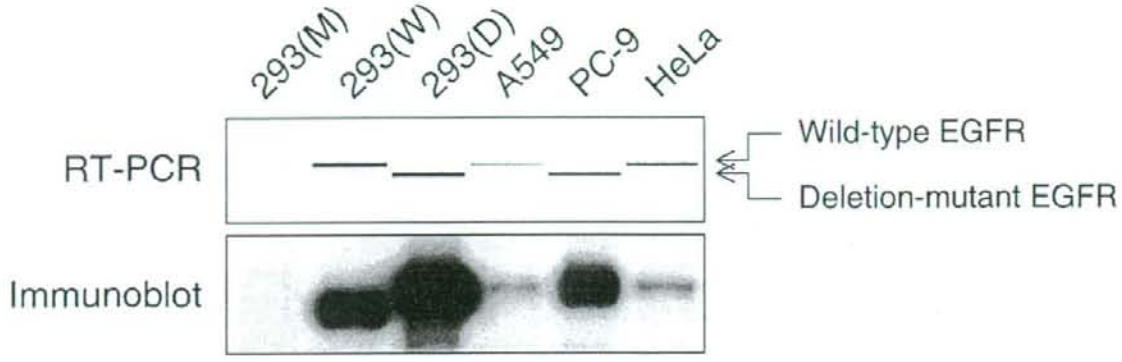

Figure 1. Expression status of epidermal growth factor receptor (EGFR) The EGFR expression level was determined by RT-PCR and immunoblot analysis. The RT-PCR products were analyzed with a 2100 Bioanalyzer. The level of EGFR protein expression was measured by immunoblot with anti-EGFR.

Fig. 2

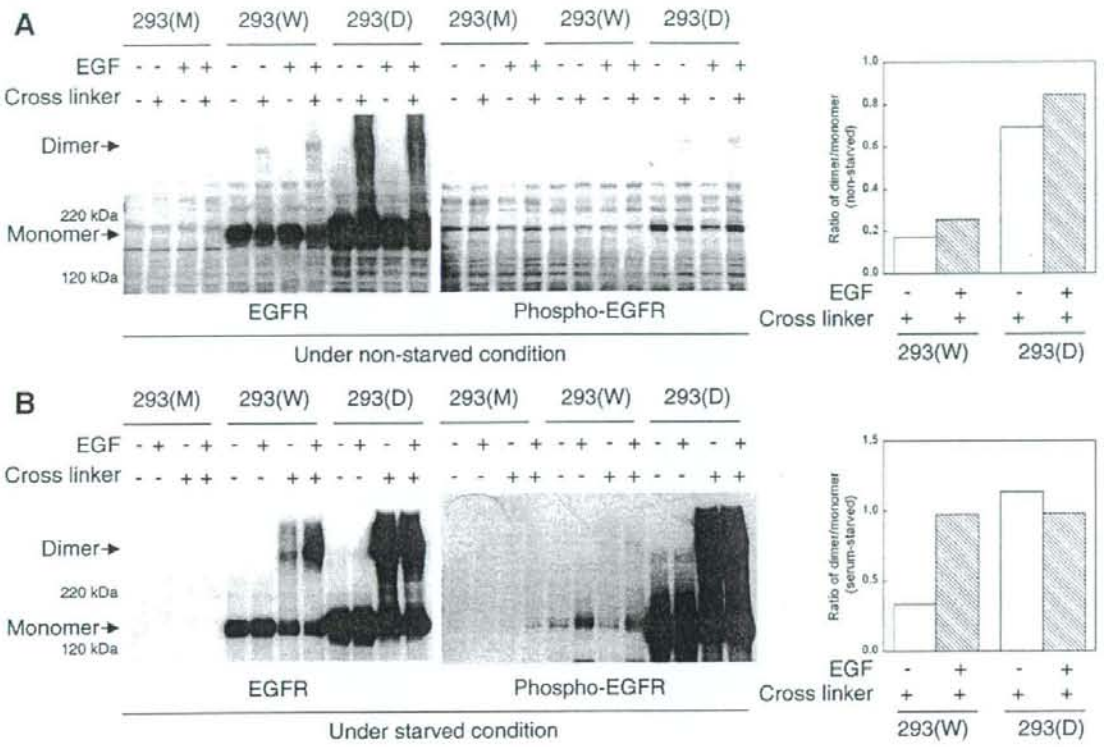

Figure 2. Dimerization and phosphorylation of wild-type EGFR and deletional EGFR. ***A***) The transfected cells were treated with or without epidermal growth factor (EGF) (10 ng/ml) for 10 min under nonstarved conditions. After two washes with ice-cold PBS(+), monolayer cells were incubated with the chemical cross-linking reagent BS^3 in PBS(+) as described in the Materials and Methods. Equivalent amounts of protein were separated by 2–15% gradient SDS-PAGE and subjected to immunoblot analysis to detect EGFR and phospho-EGFR. The ratio of dimerized to monomeric EGFR is shown in the ***right panel***. ***B***) The transfected cells were exposed or unexposed to EGF (10 ng/ml) for 10 min after serum starvation. Chemical cross-linking and immunoblotting were performed as described above. The ratio of dimerized to monomeric EGFR is shown in the ***right panel***.

Fig. 3

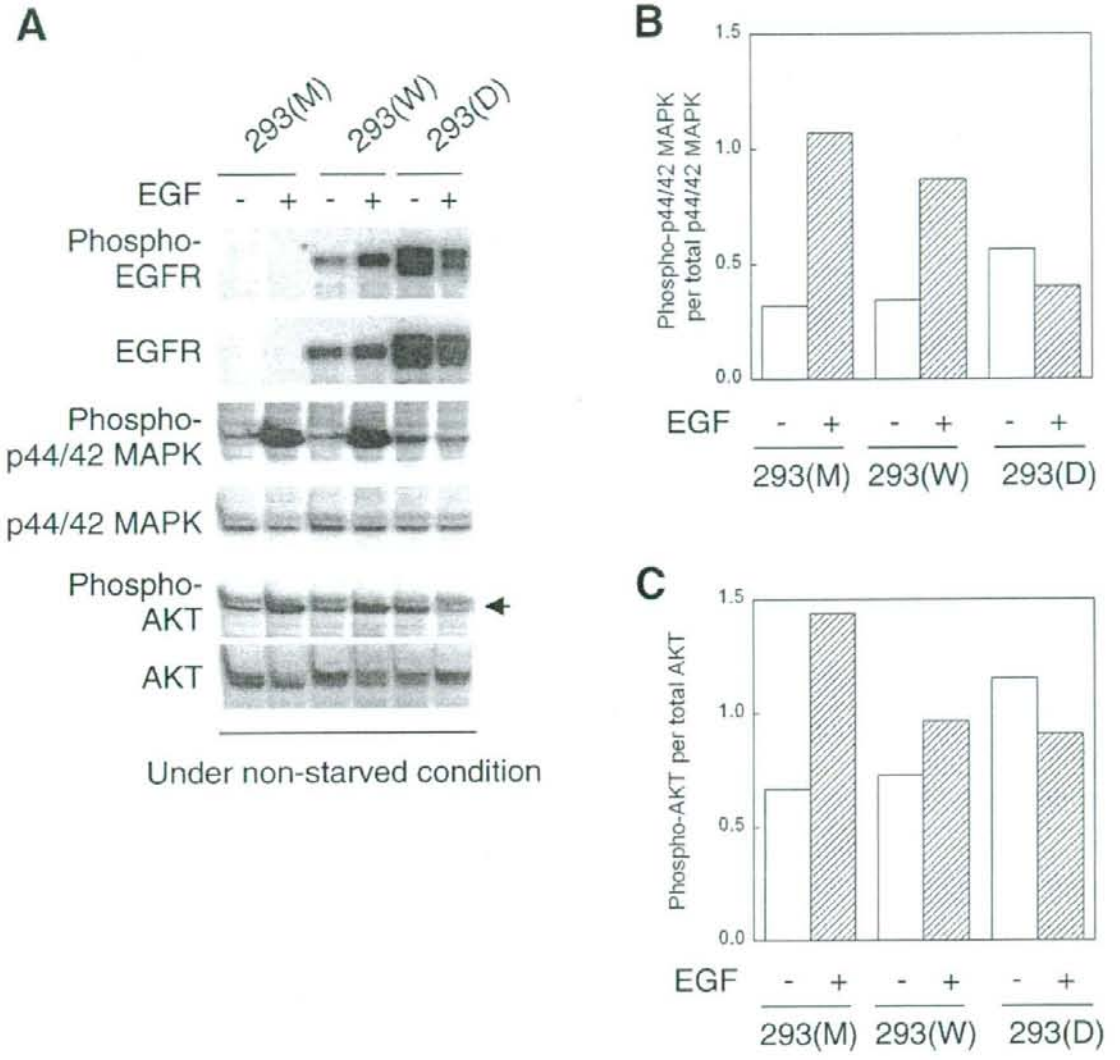

Figure 3. Phosphorylation of EGFR, p44/42 mitogen-activated protein kinase (MAPK), and AKT in the EGFR-transfected 293 cells. *A*) The 293 (M), 293(W), and 293(D) cells were treated with EGF (10 ng/ml) for 10 min under nonstarved conditions. After two washes with ice-cold PBS(+), monolayer cells were lysed. Equivalent amounts of protein were separated by 2–15% gradient SDS-PAGE for EGFR or 10–20% for p44/42 MAPK, phospho-p44/42 MAPK, AKT, and phospho-AKT, and then subjected to immunoblot analysis. *B*) Histogram of the degree of p44/42 MAPK activation expressed as phospho-p44/42 MAPK per total p44/42 MAPK. *C*) Histogram of the degree of AKT activation expressed as phospho-AKT per total AKT.

Fig. 4

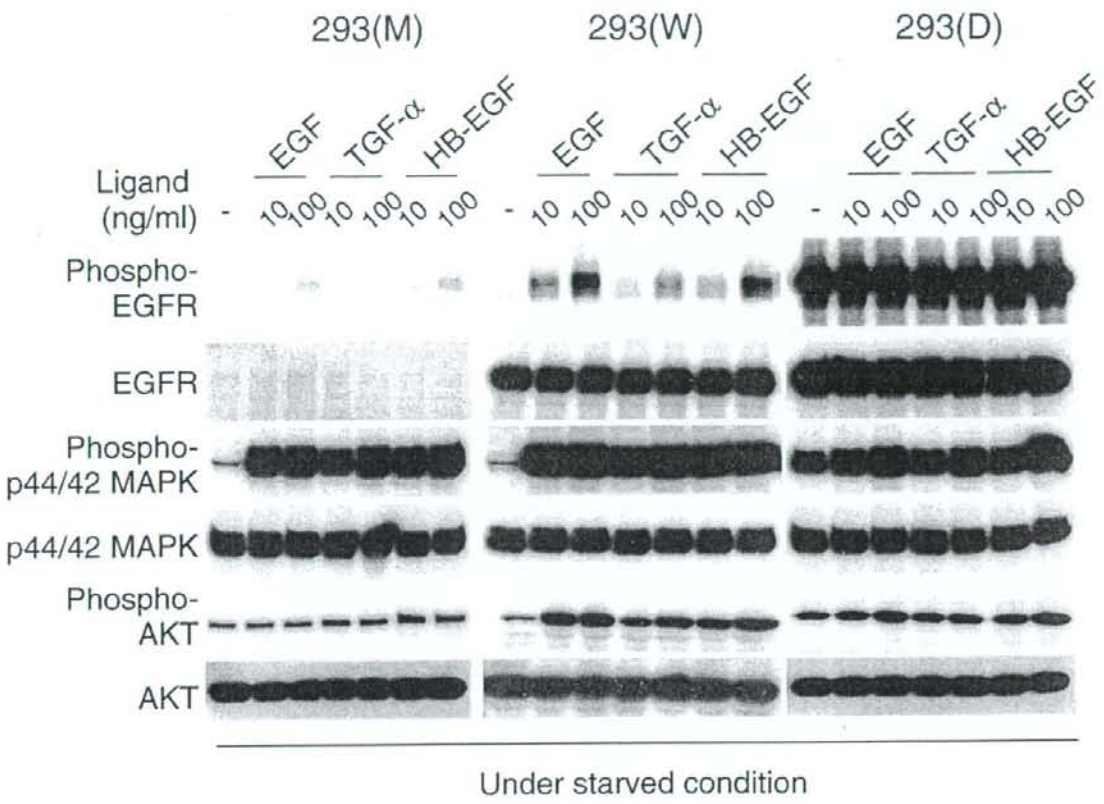

Figure 4. Phosphorylation of EGFR, p44/42 MAPK, and AKT by other ligands. The transfected cells were exposed or not exposed to EGF, TGF-α, and HB-EGF for 10 min under serum-starved conditions. After two washes with ice-cold PBS(+), monolayer cells were lysed. Equivalent amounts of protein were separated by 2–15% gradient SDS-PAGE for EGFR or 10–20% for p44/42 MAPK, phospho-p44/42 MAPK, AKT, and phospho-AKT, and then subjected to immunoblot analysis.

Fig. 5

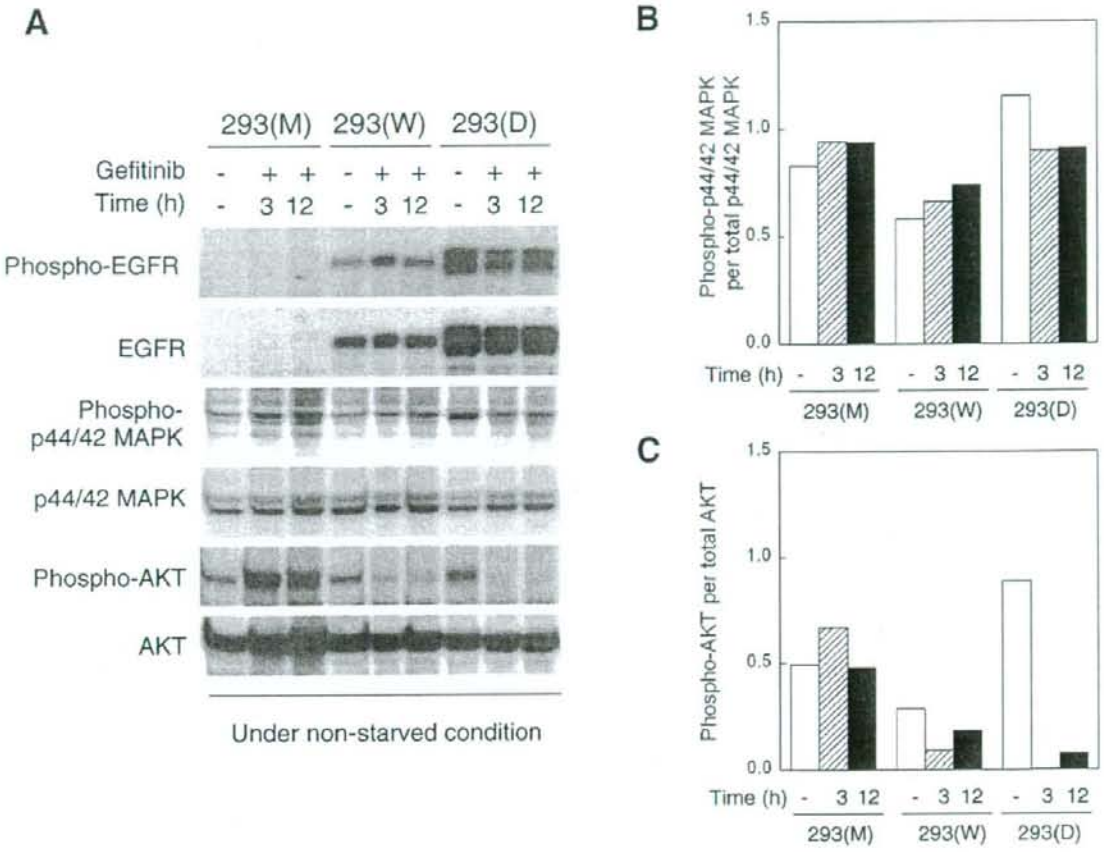

Figure 5. Effect of gefitinib on phosphorylation of EGFR, p44/42 MAPK, and AKT in the EGFR-transfected 293 cells under nonstarved conditions. ***A***) The 293(M), 293(W), and 293(D) cells were incubated with gefitinib (0.01 μM) for 3 h or 12 h under nonstarved conditions. After two washes with ice-cold PBS(+), monolayer cells were lysed. Equivalent amounts of protein were separated by 2–15% gradient SDS-PAGE for EGFR or 10–20% for p44/42 MAPK, phospho-p44/42 MAPK, AKT, and phospho-AKT, and then subjected to immunoblot analysis. ***B***) Histogram of the degree of p44/42 MAPK activation expressed as phospho-p44/42 MAPK per total p44/42 MAPK. ***C***) Histogram of the degree of AKT activation expressed as phospho-AKT per total AKT.

Fig. 6

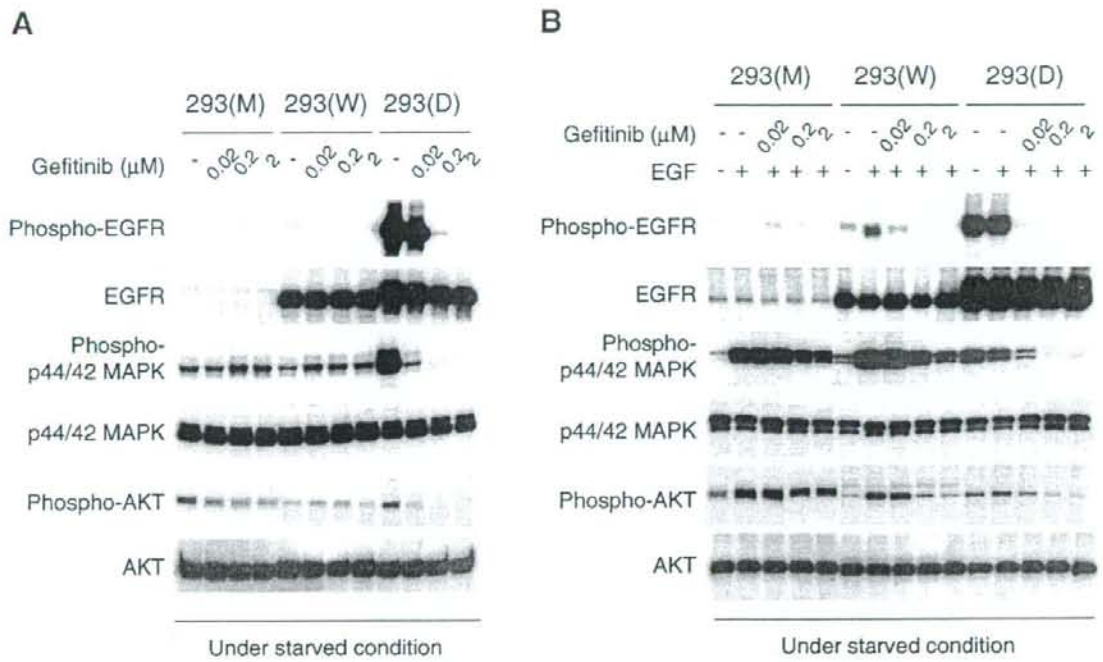

Figure 6. Effect of gefitinib on phosphorylation of EGFR, p44/42 MAPK, and AKT in the EGFR-transfected 293 cells under serum-starved conditions. ***A***) The 293(M), 293(W), and 293(D) cells were incubated with gefitinib (0.02, 0.2, 2 μM) for 3 h under serum-starved conditions. After two washes with ice-cold PBS(+), monolayer cells were lysed. Equivalent amounts of protein were separated by 2–15% gradient SDS-PAGE for EGFR or 10–20% for p44/42 MAPK, phospho-p44/42 MAPK, AKT, and phospho-AKT, and then subjected to immunoblot analysis. ***B***) The transfected cells were incubated with gefitinib (0.02, 0.2, 2 μM) for 3 h under serum-starved conditions and stimulated with EGF (100 ng/ml) for 10 min. Immunoblot analysis was performed as described above.

Fig. 7

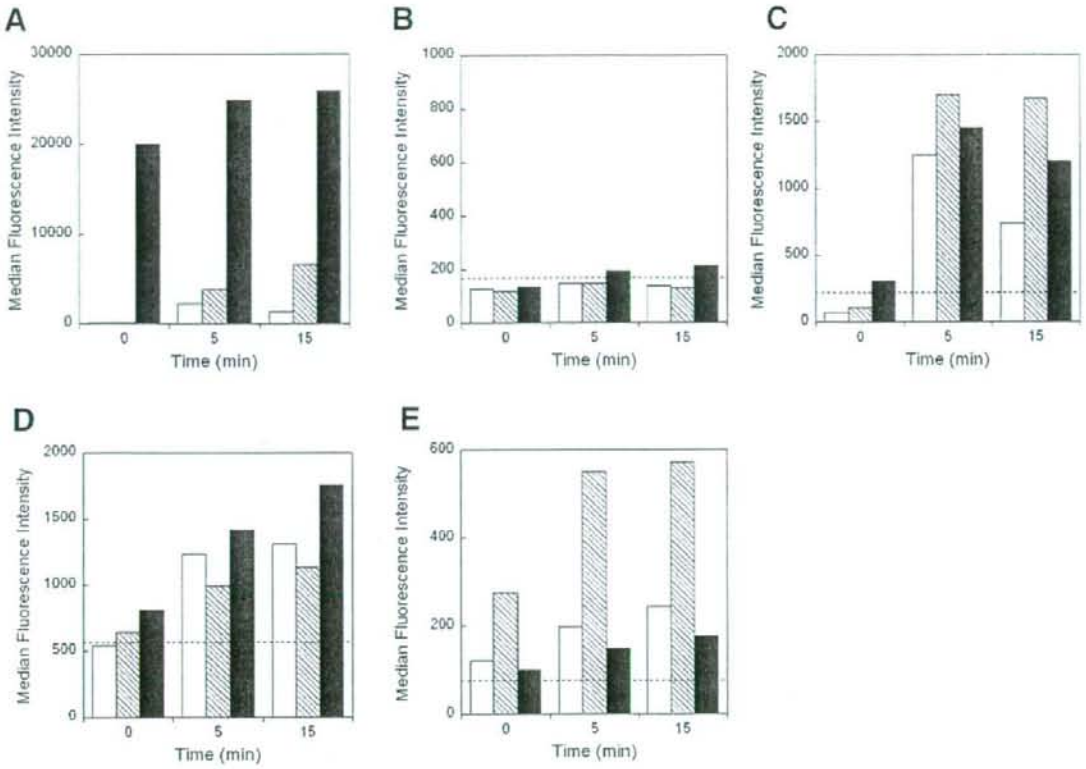

Figure 7. Monitoring of phosphoproteins after EGF stimulation in the EGFR-transfected 293 cells. The phosphoproteins in the 293(M) (open bars), 293 (W) (hatched bars), and 293(D) (solid bars) cells were analyzed by bead-based multiplex assay at the indicated intervals after addition of EGF (100 ng/ml) under serum-starved conditions. After two washes with ice-cold PBS(+), monolayer cells were lysed. The fluorescence intensity of phosphoproteins in the transfected cells was counted by bead-based multiplex assay. ***A***) phospho-EGFR; ***B***) phospho-IκB-α; ***C***) phospho-p44/42 MAPK; ***D***) phospho-ATF-2; ***E***) phospho-JNK. The dotted line shows the signal intensity of nontreated HeLa cells as a background control.

Fig. 8

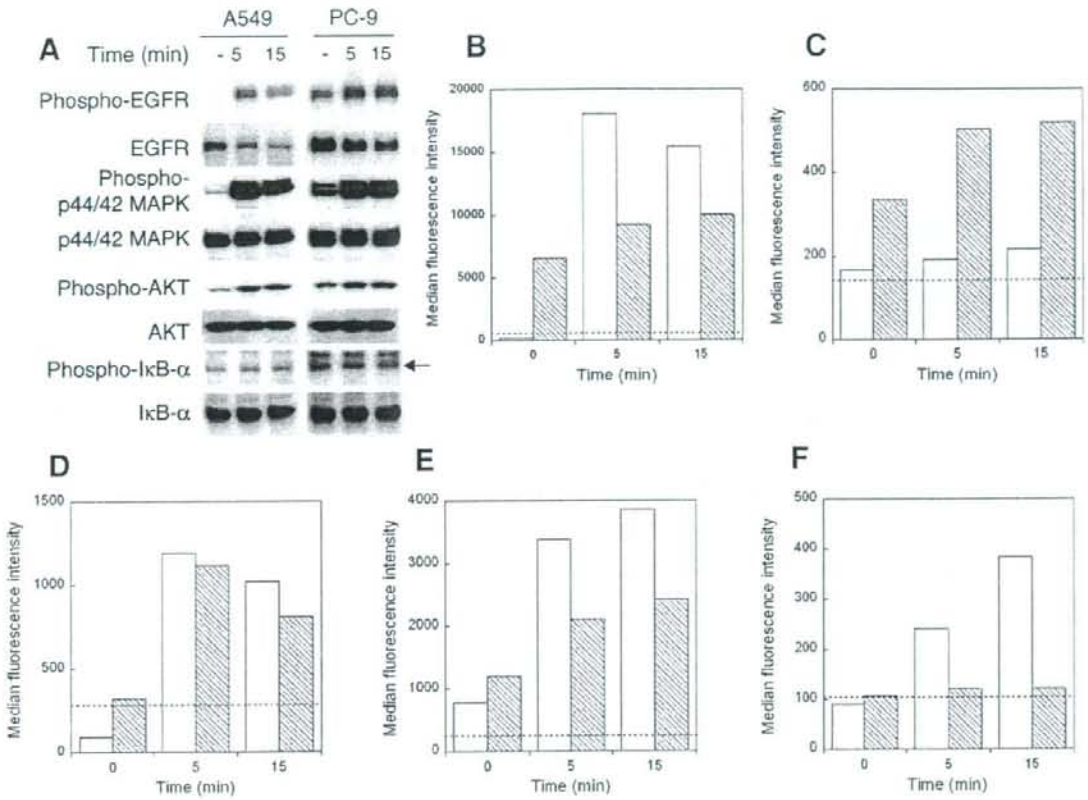

Figure 8. Monitoring of phosphoproteins after EGF stimulation in NSCLC cells. The phosphoproteins in NSCLC cells were analyzed for the indicated time intervals after addition of EGF (100 ng/ml) under serum-starved conditions. ***A***) After two washes with ice-cold PBS(+), monolayer cells were lysed. Equivalent amounts of protein were separated by 2–15% gradient SDS-PAGE for EGFR and phospho-EGFR or 10–20% for p44/42 MAPK, phospho-p44/42 MAPK, AKT, phospho-AKT, IκB-α, and phospho-IκB-α, and then subjected to immunoblot analysis. The fluorescence intensity of phosphoproteins in the A549 (open bars) and PC-9 (hatched bars) cells was counted by bead-based multiplex assay. ***B***) phospho-EGFR. ***C***) phospho-IκB-α, ***D***) phospho-p44/42 MAPK, ***E***) phospho-ATF-2, ***F***) phospho-JNK. The dotted line shows the signal intensity of nontreated HeLa cells as a background control.

Effect of the introduction of minimum lesion size on interobserver reproducibility using RECIST guidelines in non-small cell lung cancer patients

Hirokazu Watanabe,[1,6] Hideo Kunitoh,[2] Seiichiro Yamamoto,[5] Shin Kawasaki,[2] Akira Inoue,[2] Katsuyuki Hotta,[2] Kazu Shiomi,[3] Masahiko Kusumoto,[4] Kazuro Sugimura[1] and Nagahiro Saijo[2]

[1]Department of Radiology, Kobe University Graduate School of Medicine, 7-5-2 Kusunoki-cho, Chuo-ku, Kobe 650-0017; [2]Department of Medical Oncology, [3]Thoracic Surgery, and [4]Radiology, National Cancer Center Hospital; and [5]Research Center for Cancer Prevention and Screening, Statistics and Cancer Control, National Cancer Center, 5-1-1 Tsukiji, Chuo-ku, Tokyo 104-0045, Japan

(Received September 17, 2005/Revised November 24, 2005/Accepted November 28, 2005/Online publication February 16, 2006)

We evaluated interobserver reproducibility for the response evaluation criteria in solid tumors (RECIST) guidelines and the influence of minimum lesion size (MLS) on reproducibility. The 110 consecutive patients with non-small cell lung cancer were treated with platinum-based chemotherapy. Five observers measured target lesions according to both the World Health Organization (WHO) criteria and RECIST. The percentage changes for unidimensional measurements (UD; RECIST type) and bidimensional measurements (BD; WHO type) were calculated for each patient. Interobserver reproducibility among five observers, that is 10 pairs, was expressed as the Spearman's correlation coefficient for the percentage changes, the proportion of agreement and the kappa statistics for response categories. The same analysis was carried out using MLS. BD was more reproducible than UD (Spearman rank correlation coefficient, 0.84 vs 0.81; proportion of agreement, 84.4% vs 82.5%; kappa value, 0.69 vs 0.61). When MLS was applied to UD, eligible cases decreased by 6.4% and the number of target lesions by 44.6%, whereas interobserver reproducibility for UD improved (Spearman rank correlation coefficient, 0.81–0.84; proportion of agreement, 82.5–84.2%; kappa value, 0.61–0.65). The introduction of MLS to UD could also improve intercriteria reproducibility between WHO and RECIST. It is important to apply the MLS when using RECIST for the comparable interobserver reproducibility attained with WHO. (*Cancer Sci* 2006; 97: 214–218)

Tumor response to chemotherapy was previously evaluated using the WHO criteria, which stipulate bidimensional measurement (BD; WHO type) of lesions.[1] With these standardized criteria for evaluating tumor response, valid and reproducible results could be obtained by all investigators. However, a number of modifications to the WHO criteria have been developed by different institutions, which made it difficult to compare response rates for screening new anticancer agents across different investigators. This has led to the introduction of a new system, the RECIST guidelines,[2] which have been widely accepted as the new standard.

In order to standardize the methodology for evaluating tumor response, RECIST simplified the response evaluation through the use of unidimensional measurements (UD; RECIST type) instead of the BD used by the WHO criteria. Furthermore, the MLS allowable for measurement at baseline study was defined as being no less than double the slice thickness on CT or MRI.

The validity and intercriteria reproducibility between the new RECIST guidelines and the previous WHO criteria have been investigated.[2–7] However, to the best of our knowledge, no analysis of the influence of MLS on interobserver reproducibility, specified for measurability in tumor response evaluation according to the RECIST guidelines, has been published in the literature.

The purpose of the present study was therefore to evaluate interobserver reproducibility in tumor response evaluation using RECIST, intercriteria reproducibility between WHO and RECIST, and whether this reproducibility is affected by the application of MLS.

Materials and Methods

Patient population

This is a retrospective study of the radiological findings for patients who underwent chemotherapy for advanced NSCLC. The subjects were patients treated during clinical trials at the Medical Oncology Division of the National Cancer Center Hospital in Tokyo, Japan, between January 1999 and January 2001. All clinical trials were conducted in accordance with the Helsinki Declaration and the protocols were approved by the institutional review board. Written informed consent was obtained from each patient for the treatment protocols, which included the secondary use of treatment-associated documents. Patients were staged according to the Union Internationale Contra le Cancer TNM classification of malignant tumors.[8] The 110 eligible patients included those histologically or cytologically diagnosed with NSCLC. Patients were required to undergo CT scans periodically for evaluating tumor response prior to and once after

[6]To whom correspondence should be addressed. E-mail: h-watanabe@kcc.zaq.ne.jp
Abbreviations: BD, bidimensional measurements; CR: complete response; CT, computed tomography; MLS, minimum lesion size; MRI, magnetic resonance imaging; NSCLC, non-small cell lung cancer; PD, progressive disease; PR, partial response; RECIST, response evaluation criteria in solid tumors; SD, stable disease; TNM, tumor node metastases; UD, unidimensional measurements; WHO, World Health Organization.

doi: 10.1111/j.1349-7006.2006.00157.x

treatment, to have at least one bidimensionally measurable lesion, and to be treated with chemotherapy in clinical trials.

Patients treated in clinical practice were considered to be unsuitable and excluded from this study as tumor response evaluation in the clinical practice of oncology is not always carried out according to predefined criteria, but rather is made by subjective medical judgment based on clinical and laboratory data. In addition, tumor response evaluation is not always carried out by CT examination, and the intervals between tumor evaluations can be irregular.

Image analysis

Almost all images were acquired with a TCT-900S Superhelix (Toshiba Medical, Tokyo, Japan), with the remainder scanned on an X-Vigor helical CT scanner (Toshiba Medical). Helical CT was carried out with fixed scanning parameters, including a table speed of 15 mm/s, a pitch ratio of 1:1.5 per rotation time 1 s, and the same contrast agent for both baseline and follow-up evaluations. Image reconstruction was carried out at intervals of 10 mm.

On chest CT obtained during baseline examination before the initiation of chemotherapy, target lesions up to a maximum of five lesions per patient with longest and perpendicular diameters that could be measured accurately were selected by one diagnostic radiologist. In addition, one follow-up chest CT examination, indicating tumors with the greatest response to chemotherapy, was selected retrospectively. Target lesions included primary lung lesion, pulmonary metastases and lymph nodes.

For the target lesions, the two parameters consisting of the longest diameter and the diameter perpendicular to it were measured with electronic calipers on digitized images. Five observers of different backgrounds, blinded to patient profiles, reviewed all patients independently and no attempt was made to arrive at a consensus. These observers included one diagnostic radiologist, one thoracic physician, two medical oncologists and one thoracic surgeon.

Tumor response evaluation

The sum of the longest diameters for all target lesions was calculated for pretreatment and post-treatment UD. Similarly, the sum of the products of the longest diameters and their perpendicular diameters for all target lesions was calculated for pretreatment and post-treatment BD. If there were two or more lesions, the sum of all target lesions was calculated. The baseline sum was used as the reference from which objective tumor response could be calculated. The percentage changes were calculated as post-treatment value divided by pretreatment value for both UD and BD.

Percentage changes were then classified using the current RECIST guidelines and the previous WHO criteria tumor response classification system. Tumor response was categorized into CR, PR, SD and PD based on both RECIST guidelines and WHO criteria. The RECIST PR was defined as a 50% decrease in the percentage changes for UD, and the WHO PR was defined as a 30% decrease in the percentage changes for BD. The RECIST PD was defined as a 20% increase in the sum of the longest diameters, and the WHO PD was defined as a 25% increase in the sum of the products of the two diameters of all lesions or in the product of the diameters of one lesion. For the present study, no minimum interval was required for the confirmation of either CR or PR.

Analysis of intercriteria reproducibility

To examine intercriteria reproducibility, the mean and ranges of differences in the response rate between UD and BD were calculated. We then estimated those between UD-MLS and BD. Interobserver differences among the five observers yielded 20 pair comparisons. Intraobserver differences of the same observer yielded five pair comparisons.

Analysis of interobserver reproducibility

First, to examine the interobserver reproducibility of the percentage changes according to the two different dimensional measurements, we estimated the Spearman's correlation coefficient of the percentage changes among the five observers, calculated for each pair observed (five observers yielded 10 pair comparisons).

Second, to examine the interobserver reproducibility for two tumor response criteria, we estimated the proportion of agreement to the categories of CR, PR, SD and PD for both UD and BD among the five observers (10 pair comparisons). We then calculated the kappa statistics, a measure of agreement in which agreement is taken into consideration by chance, to assess interobserver reproducibility for tumor response categories.[9]

Third, we examined the influence of MLS on the number of eligible cases and target lesions. The same analyses on interobserver reproducibility were conducted applying the MLS. MLS was introduced into the RECIST guidelines, which specify a minimum lesion size of less than double the slice thickness on images. The slice thickness was 10 mm in the present study, so the MLS was set at no less than 20 mm at baseline evaluation before treatment. Cases that only had tumors smaller than the MLS were excluded from the present study. We defined the RECIST guidelines as the evaluation by UD for measurable cases and the WHO criteria as the evaluation by BD for all cases.

SAS version 8.02 (SAS Institute, Cary, NC, USA) was used for all analyses.

Results

Patient population

The characteristics of the 110 patients were as follows: male/female = 80/30, median age = 59 years (range 36–72 years), stage IIIB/IV = 33/77. Chemotherapy regimens are listed in Table 1. A total of 220 CT images were reviewed, comprising 110 CT images each from the baseline study (pretreatment) and from the follow-up (post-treatment) study.

Tumor response evaluation between UD and BD

The tumor response evaluation was categorized into CR, PR, SD and PD without MLS. The response rate results are shown in Table 2. None of the patients were rated CR. The use of UD resulted in response categories by observers A, B, C, D and E of 35, 28, 26, 34 and 36 PR, 73, 79, 81, 73 and 71 SD, and 2, 3, 3, 3 and 3 PD, respectively. The response rate ranged from 23.6 to 32.7%. For BD, the corresponding response categories were 37, 30, 33, 36 and 36 PR, 67, 73,

Table 1. Characteristics of the 110 patients enrolled in the present study

Characteristic	n
No. patients	110
Age (years)	
Median	59
Range	36–72
Sex	
Male	80
Female	30
Disease stage at study entry	
IIIB	33
IV	77
Tumor histology	
Adenocarcinoma	78
Squamous	22
Large-cell	1
Unclassified non-small cell	9
Regimen	
Cisplatin and gemcitabine	21
Cisplatin and paclitaxel	18
Nedaplatin and paclitaxel	15
Cisplatin and vinorelbine	14
Carboplatin and paclitaxel	14
Cisplatin and vindesine	13
Cisplatin, docetaxel and ifosfamide	7
Cisplatin and docetaxel	8

Table 2. Response rate (%) using four different measurements among five observers

Measurement	Observer					Mean
	A	B	C	D	E	
UD	31.8	25.5	23.6	30.9	32.7	28.9
BD†	33.6	27.3	30.0	32.7	32.7	31.3
UD-MLS‡	33.0	27.2	32.0	30.1	32.0	30.9
BD-MLS	35.0	32.0	33.0	33.0	34.0	33.4

†WHO criteria; ‡RECIST guidelines. BD, bidimensional measurement; MLS, minimum lesion size; UD, unidimensional measurement.

68, 68 and 68 SD, and 6, 7, 9, 6 and 6 PD, respectively. The response rate ranged from 27.3 to 33.6%.

Tumor response evaluation between UD-MLS and BD-MLS

When the MLS criteria were applied, the number of eligible cases decreased by 6.4% from 110 to 103, and the number of target lesions decreased by 44.6% from 402 to 223.

The response rate results are shown in Table 2. None of the patients were rated CR. When UD was used with MLS, the respective response evaluations made by observers A, B, C, D and E were 34, 28, 33, 31 and 33 PR, 68, 73, 67, 72 and 68 SD, and 1, 2, 3, 0 and 2 PD. The response rates of UD applying MLS ranged from 27.2 to 33.0%, showing a reduction in interobserver difference compared with those of UD not applying MLS. With BD using the MLS, the corresponding response categories were 36, 33, 34, 34 and 35 PR, 63, 66, 65, 63 and 64 SD, and 4, 4, 4, 6 and 4 PD. The response rate ranged from 32.0 to 35.0%.

Intercriteria reproducibility

The intercriteria reproducibility in the response rates is shown in Table 3. Between UD and BD, the intraobserver difference in the response rates ranged from 0 to 6.4% with a mean of 2.36%, and the interobserver difference ranged from 0 to 10.0% with a mean of 4.25%. Between UD-MLS and BD, the intraobserver difference in the response rates ranged from 0.1 to 2.6% with a mean of 1.26%, and the interobserver difference ranged from 0.1 to 6.4% with a mean of 2.76%.

Correlations between UD and BD

The mean and ranges of interobserver reproducibility among five observers using the two dimensional measurements are shown in Table 4. The mean value of the Spearman rank correlation coefficient for the percentage changes when using UD (0.81) was lower than that using BD (0.85), and the same tendency was observed for the mean value of proportion of agreement for the tumor response categories (82.5%, 908/1100 vs 84.4%, 928/1100) and the mean kappa statistics for the tumor response categories (0.61 vs 0.69). The lowest kappa statistics among the 10 pair comparisons were 0.49 with UD and 0.61 with BD. The kappa statistics obtained with BD were higher than those with UD in nine out of 10 pair comparisons (Fig. 1).

Correlations between UD and UD-MLS

The mean values and ranges of interobserver reproducibility when applying the MLS are shown in Table 4. The mean value of Spearman's correlation coefficient for UD-MLS (0.84) was higher than that for UD (0.81), and the same tendency was observed for the mean value of proportion of agreement for the tumor response categories (84.2%, 867/1030 vs 82.5%, 908/1100) and the mean kappa statistics for the tumor response categories (0.65 vs 0.61). The lowest kappa statistics among the 10 pair-based comparisons was 0.57 with MLS and 0.49 without. When MLS was used together with UD, the kappa statistics increased in eight out of 10 pair comparisons (Fig. 2).

Table 3. Intercriteria reproducibility: difference in the response rate (%) among five observers

Category	UD and BD†		UD-MLS‡ and BD†	
	Mean	Range	Mean	Range
Overall (25 comparisons)	3.87	0–10	2.45	0.1–6.4
Interobserver (20 comparisons)	4.25	0–10	2.76	0.1–6.4
Intraobserver (5 comparisons)	2.36	0–6.4	1.26	0.1–2.6

†WHO criteria; ‡RECIST guidelines. BD, bidimensional measurement; MLS, minimum lesion size; UD, unidimensional measurement.

doi: 10.1111/j.1349-7006.2006.00157.x

Table 4. Interobserver reproducibility (10 pair comparisons) using four different measurements among five observers

Category	No. patients	Spearman's correlation coefficient		Proportion of agreement (%)		Kappa statistic	
		Mean	Range	Mean	Range	Mean	Range
UD	110	0.81	0.76–0.86	82.5	77.3–89.1	0.61	0.49–0.75
BD[†]	110	0.85	0.79–0.89	84.4	80.0–89.1	0.69	0.61–0.78
UD-MLS[‡]	103	0.84	0.75–0.89	84.2	80.6–88.3	0.65	0.57–0.73
BD-MLS	103	0.86	0.80–0.89	84.0	78.6–89.3	0.68	0.58–0.78

[†]WHO criteria; [‡]RECIST guidelines. BD, bidimensional measurement; MLS, minimum lesion size; UD, unidimensional measurement.

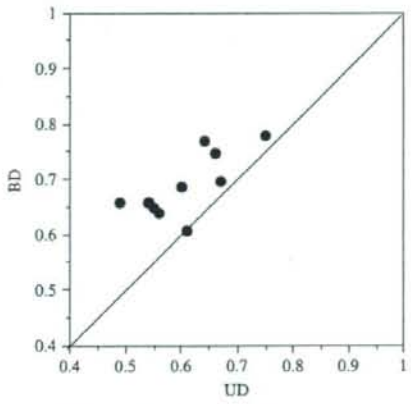

Fig. 1. Scattergram showing the kappa statistics for the use of unidimensional (UD) and bidimensional (BD) measurements. The kappa values for BD were higher than those for UD in nine of 10 pair comparisons.

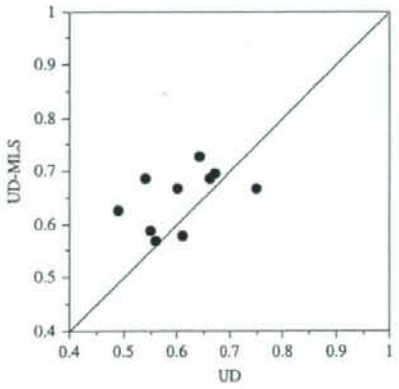

Fig. 2. Scattergram showing the kappa statistics for the use of unidimensional measurement (UD) and UD with minimum lesion size (MLS). When MLS was applied to UD, the kappa values increased in eight of 10 pair comparisons.

Discussion

Standardized tumor response evaluation systems are considered reliable in clinical trials when they are valid and reproducible among different observers. Although the intercriteria reproducibility between the new RECIST guidelines and the previous WHO criteria had been investigated,[2–7] little information was available concerning interobserver reproducibility of tumor response evaluation. In addition, statistical analysis results regarding the effect of MLS on interobserver reproducibility had not been provided in previous reports. This is the first study to investigate interobserver reproducibility of the RECIST guidelines evaluating the MLS.

The importance of interobserver reproducibility for any classification scheme has been discussed previously for other grading systems.[10–12] Clinical investigators must take into account interobserver reproducibility in tumor response evaluation, which can greatly affect the results in clinical trials. Our findings demonstrated that interobserver variability exists for bidimensional measurements, as in studies published previously.[13,14] For example, Hopper *et al.* showed considerable interobserver variability in CT tumor measurements between radiologists interpreting thoracic and abdominal/pelvic CT scans.[13] In another report, the impact of an evaluation committee on patients' overall response status in a large multicenter trial in oncology was evaluated.[14] Major disagreements occurred in 40% of cases and minor disagreements occurred in 10.5% of the cases reviewed. The number of responders was reduced by 23.2% after review by the evaluation committee.

The range of response rates among five observers was clearly narrowed by the MLS (Table 2). The response rates assessed by UD varied from 23.6 to 32.7%. When assessed by BD, the response rates ranged from 27.3 to 33.6%. Response rates assessed with UD-MLS ranged from 27.2 to 33.0%, which was almost identical when BD was used.

The results of the present study also suggested that BD was more reproducible than UD. When MLS was applied to UD, the mean values and ranges of Spearman's correlation coefficient, proportion of agreement and the kappa statistics improved (Table 4). In order to ensure comparable interobserver reproducibility (as was originally achieved with the WHO criteria) it is essential that the MLS be used in combination with UD when using RECIST.

Because of the need to retain some ability to compare results of future therapies with those available currently, no major discrepancy should exist between the old (WHO) and